Extrinsic ion migration in perovskite solar cells

Zhen Li,[1] Chuanxiao Xiao,[1, 2] Ye Yang,[1] Steve Harvey,[1] Dong Hoe Kim,[1] Jeffrey A. Christians,[1] Mengjin Yang,[1] Philip Schulz,[1] Sanjini U. Nanayakkara,[1] Chun-Sheng Jiang,[1] Joseph M. Luther,[1] Joseph Berry,[1] Matthew C. Beard,[1] Mowafak M. Al-Jassim,[1] Kai Zhu[1,]*

1. National Renewable Energy Laboratory, Golden, Colorado 80401, USA
2. Colorado School of Mines, Golden, CO 80401, USA

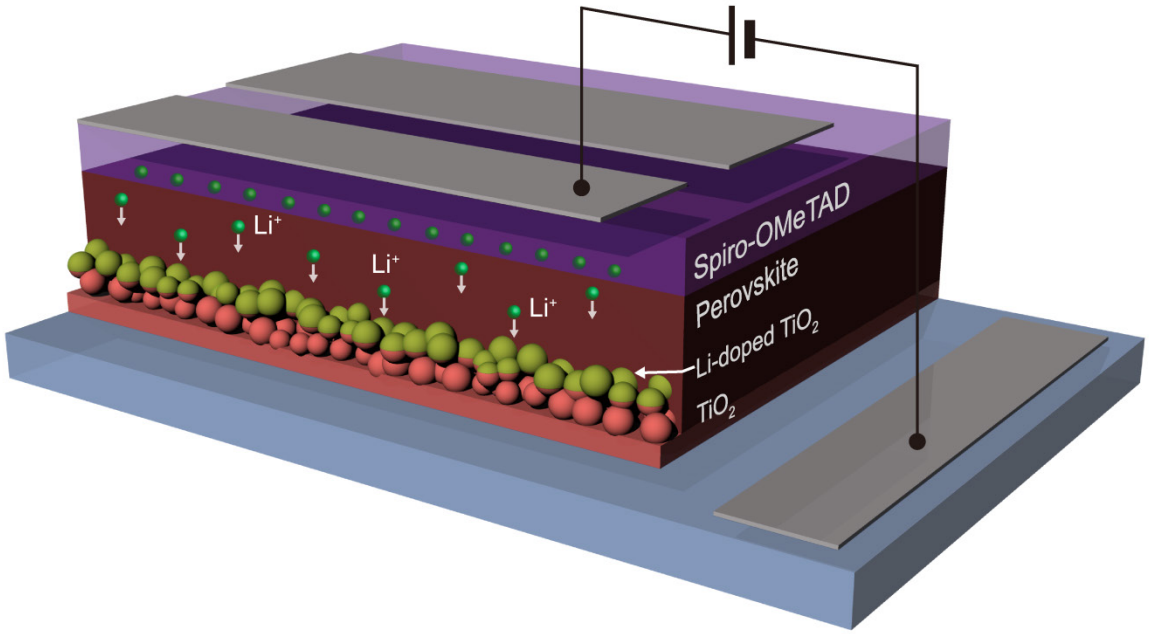

Extrinsic ions (e.g., Li^+) migrate across perovskite solar cell and modify TiO_2 layer, affecting device performance and hysteresis.

Abstract

The migration of intrinsic ions (e.g., MA^+, Pb^{2+}, I^-) in organic-inorganic hybrid perovskites has received significant attention with respect to the critical roles of these ions on the hysteresis and degradation in perovskite solar cells (PSCs). Here, we demonstrate that extrinsic ions (e.g., Li^+, H^+, Na^+), when used in the contact layers in PSCs, can migrate across the perovskite layer and strongly impact PSC operation. In a TiO_2/perovskite/spiro-OMeTAD-based PSC, Li^+-ion migration from spiro-OMeTAD to perovskite and TiO_2 layer is illustrated by time-of-flight secondary-ion mass spectrometry. The movement of Li^+ ions in PSCs plays an important role in modulating the solar cell performance, tuning TiO_2 carrier-extraction properties, and affecting hysteresis in PSCs. The influence of Li^+-ion migration was investigated using time-resolved photoluminescence, Kelvin probe force microscopy, and external quantum efficiency spectra. Other extrinsic ions such as H^+ and Na^+ also show a clear impact on the performance and hysteresis in PSCs. Understanding of the impacts of extrinsic ions in perovskite-based devices could lead to new material and device designs to further advance perovskite technology for various applications.

Introduction

Organic-inorganic hybrid perovskite materials have recently drawn tremendous interest due to their potential for constructing high-performance solar cells[1, 2] and optoelectronic devices[3-5] with low-cost and low-energy solution processing.[6, 7] The research enthusiasm is largely a result of the rapidly rising power conversion efficiencies (*PCE*s) of solid-state perovskite solar cells (PSCs), surging from single digits to over 22% within four years.[8-10] Hybrid perovskites have many ideal characteristics as photovoltaic (PV) materials, such as high absorption coefficient, long carrier diffusion length, and low density of trapping states.[11-14] However, unlike most of the traditional PV materials, the hybrid perovskites materials (e.g., $CH_3NH_3PbI_3$ or $MAPbI_3$) show very strong ionic characteristics.[15] Numerous reports with both theoretical calculations[16-18] and experimental observations[19-22] show that the ions in perovskite materials (e.g., MA^+ or I^-) have low activation barriers to movement and modest ionic diffusion coefficients to move within perovskite devices, especially when subjected to external bias or under light illumination. This feature of hybrid perovskites has inspired many exciting studies leading to novel optoelectronic/electronic applications, such as switchable PV[23] and nonvolatile memory.[24, 25] However, it has also led to slow changes of optoelectronic properties and performances in perovskite-based devices on timescales of seconds to minutes. This was initially noticed through the anomalous current density-voltage (*J-V*) hysteresis in the PSCs[26] and subsequently evidenced by more phenomena such as solar cell performance modulation by pre-condition biasing and light soaking,[27-29] slow photoconductivity response,[30] and halide redistribution and segregation.[31, 32] Furthermore, ionic movement has adverse effects on stability of PSCs because the migrating ions can react with metal electrodes[33] and not return to the equilibrium position after electrical poling, resulting in degradation of PSCs. Thus, understanding and controlling the ionic movements in perovskite materials is critical for perovskite-based electronic and optoelectronic applications.

The discrepancy of *J-V* curves when scanned at forward and reverse directions—so-called *J-V* hysteresis—is one of the obstacles hindering the commercialization of PCSs, due to the unstable PV output and difficulty in precisely determining the PV performance parameters.[34] Several mechanisms have been suggested as origins of *J-V* hysteresis in PSCs such as ferroelectric polarization,[35] trapping of carriers at interfaces[36] and capacitive current induced

by ion redistribution.[37] However, the leading explanation is ion migration and accumulation at the two charge-extraction interfaces that modulate the built-in electric field in PSCs.[27, 38] More recent modeling and experiments suggest that *J-V* hysteresis is a combined effect of ion migration and change of interface recombination induced by the accumulated ionic spices or defects.[39, 40] There are reports showing that ions from perovskites could move into the hole/electron transport layers (HTL/ETLs), enhance carrier-extraction ability, and reduce interface recombination, leading to reduced hysteresis.[41, 42] Regardless of the exact mechanism considered, most of studies on ion migration have been focused only on the intrinsic ions (e.g., MA^+, Pb^{2+}, and I^-) from the perovskite layer itself.[15-20, 22, 23, 29, 37-42] Extrinsic ions from the transport layers (HTLs/ETLs), such as various dopants from these layers, have been largely overlooked to date.

Here, we demonstrate the significance of extrinsic ion migration to the PSC operation. Using a common device architecture (TiO_2/perovskite/spiro-OMeTAD) as an example, we show that Li^+ ion from the spiro-based HTL can migrate across the perovskite absorber layer to reach the TiO_2 ETL. Measurements from time-resolved photoluminescence (TRPL), Kelvin probe force microscopy (KPFM), and external quantum efficiency (EQE) spectra indicate that the movement of Li^+ ions in PSCs strongly affect the solar cell performance, TiO_2 charge-extraction property, and hysteresis in PSCs. These results can be generalized to other extrinsic ions such as H^+ and Na^+. Thus, it is important to study extrinsic ion migration for better understanding of the general operation mechanisms of perovskite devices.

Results and discussion

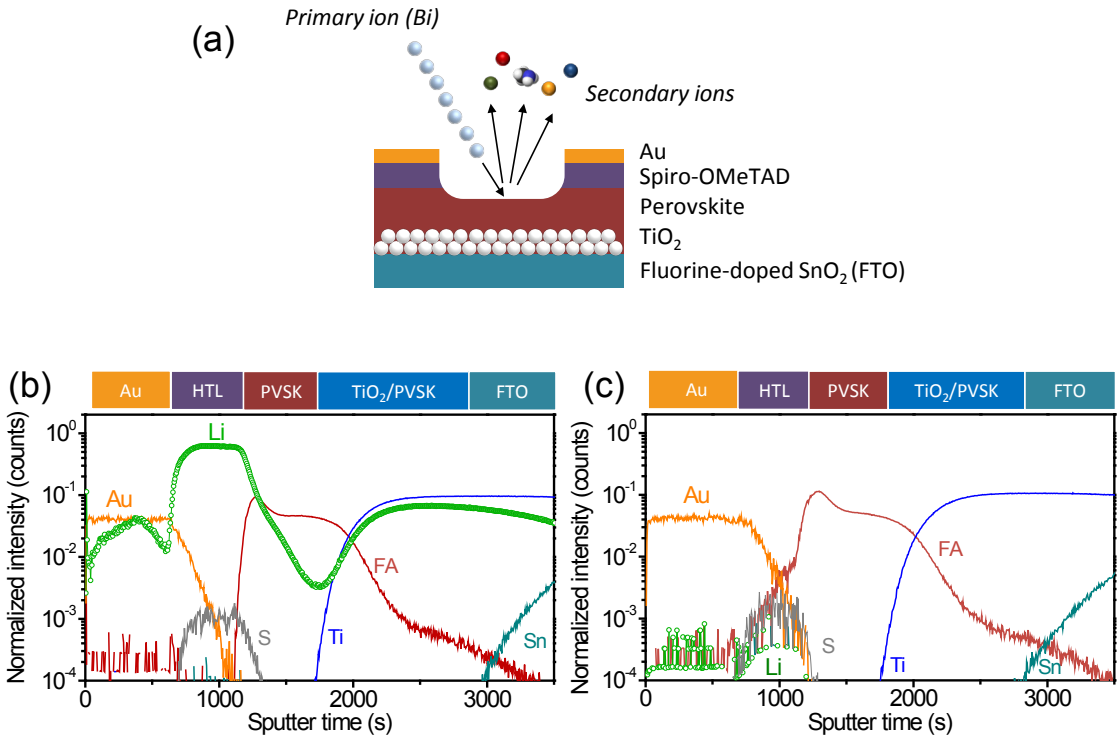

Figure 1. Elemental depth profile of PSCs with and without Li-TFSI dopant in spiro-OMeTAD layer. (a) Schematic of time-of-flight secondary-ion mass spectroscopy technique for 1-D elemental distribution analysis in PSCs; (b–c) elemental depth profile of PSC with (b) and without (c) Li-TFSI dopants, showing a broad distribution of lithium in Li-containing solar cells and a lithium signal at or below the instrument background level in the Li-free cells. The sputter time is not scaled to the actual thickness of each layer due to the different sputter rates from different layers.

The depth profiles of several key elements in PSCs determined by time-of-flight secondary-ion mass spectrometry (TOF-SIMS) is shown in **Figure 1**. TOF-SIMS can detect elements and molecular species with parts-per-million or better sensitivity, with a dynamic range of 4 orders of magnitude. Two types of PSCs were analyzed. One used spiro-OMeTAD HTL doped with pre-oxidized spiro(TFSI)$_2$ and Li-TFSI (referred to as a Li-containing cell), and a second cell used spiro-OMeTAD HTL doped with only spiro(TFSI)$_2$ (referred to as a Li-free cell). Both cells show decent PV output, which will be discussed later. The positions of the different layers through the depth profile of the entire device were estimated by detection of the dominant secondary-ion signal for the various layers. It is worth noting that the layer thickness is not in direct proportion to the sputtering time as a result of different sputtering rates of different layers, because the sputter rate is related to the bond strength of the layer (e.g., gold sputters

much slower than the HTL). The actual layer thicknesses were determined from cross-sectional scanning electron microscopy (SEM) images of the device as shown in **Figure S1**. There is apparent overlap between adjacent layers due to the roughness of each layer, probable inter-penetration of the adjacent layers, and a small artifact effect from SIMS beam mixing. In the Li-containing PSC, lithium is primarily located in the Li-doped spiro-OMeTAD HTL (which is determined using the element S from the $TFSI^-$ anions of the dopants); but there is also a significant amount of lithium found in the perovskite and TiO_2 layer, which likely results from lithium diffusion across the device stack. In contrast, the Li-free PSC shows a lithium signal at or below the instrument background in the spiro-OMeTAD layer. It is well known that the Li^+ ion is small and thus has a high diffusion tendency. The migration of Li^+ through perovskite materials has been demonstrated by using $MAPbBr_3$ and $MAPbI_3$ perovskites as anode materials in Li-ion batteries.[43] It is interesting to note that lithium concentration does not follow a simple Fixian diffusion distribution in the Li-containing PSC; it rises to a higher concentration in the TiO_2 layer than in the perovskite layer. This suggests a higher affinity of Li^+ ion to TiO_2 than to perovskite. This is consistent with the findings that the TiO_2 is also a good anode material for a Li-ion battery such that Li^+ could easily be inserted into or extracted from the TiO_2 ETL in PSCs.[44, 45] These TOF-SIMS results show clear evidence that Li^+ ions are diffusing across the perovskite layer and entering the oxide layer. It is important to note that this Li^+-ion migration differs from the commonly studied intrinsic ion migrations in perovskite materials (e.g., MA^+ or I^-). The Li^+ ions are from an extrinsic ion source, Li-TFSI, which is used as a standard dopant for HTLs. However, the roles of extrinsic ions (such as Li^+) on PSCs have been largely overlooked.

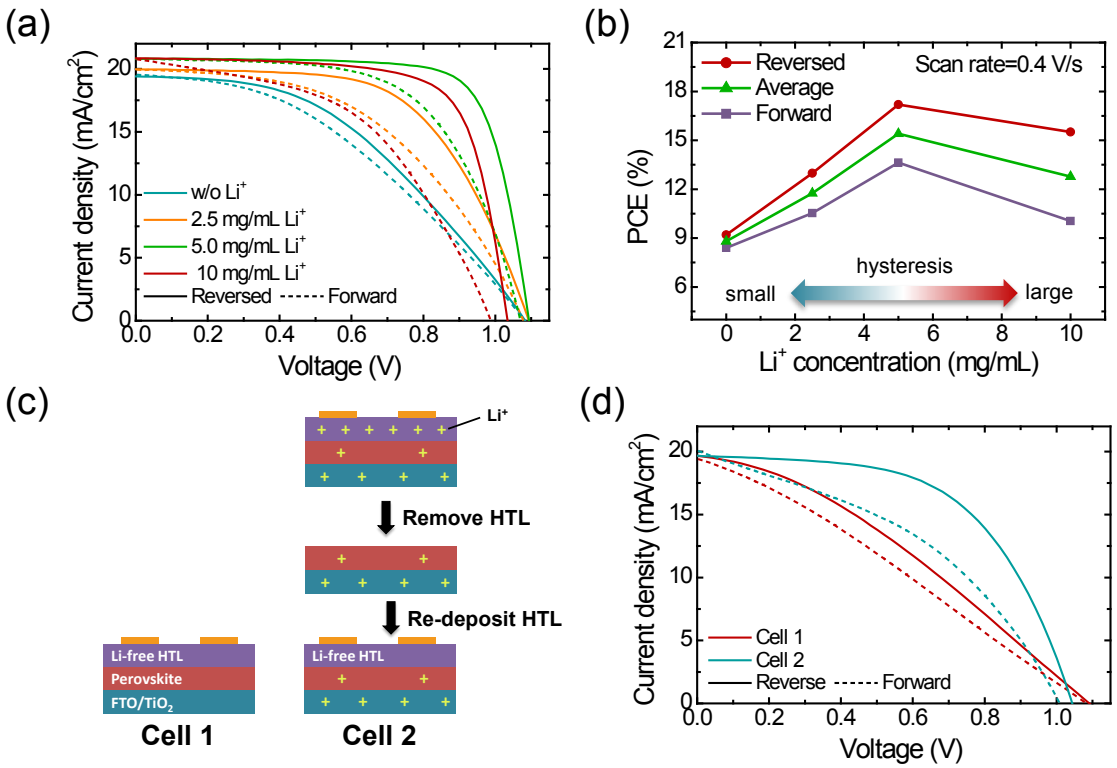

Figure 2. PSCs performance with different amount of Li-TFSI in spiro-OMeTAD HTL. (a) *J-V* curves with forward and reverse scan; (b) *PCE* with forward and reverse scan, with the green curve showing the average of forward and reverse *PCE*; (c) Schematics; and (d) *J-V* curves of solar cells with same Li-free HTL but different fabrication histories.

We examined the influence of Li^+ ions on device characteristics through PSCs with a series of Li-TFSI concentrations doped in the spiro-OMeTAD layers. The Li-free cell used pre-oxidized spiro-OMeTAD spiro$(TFSI)_2$ as the dopant,[46] whereas other cells used both spiro$(TFSI)_2$ and different amounts of Li-TFSI as the dopants. All cells were tested under AM1.5G 100-mW/cm^2 illumination with voltage swept first in forward (short-circuit current [J_{sc}] to open-circuit voltage [V_{oc}]) and then reverse (V_{oc} to J_{sc}) directions with a scan rate of 0.4 V/s. Representative *J-V* curves are shown in **Figure 2a** with each scan direction and the stable power output were shown in **Figure S7**. The statistical performance parameters of the reverse scan are tabulated in **Table 1** for PSCs with different Li-TFSI amounts. As Li-TFSI concentration in the HTL is increased from 0 to 10 mg/mL (equivalent to a Li^+/spiro molar ratio from 0 to 0.54), the fill factor (*FF*) increased monotonically from 0.48 to 0.79. V_{oc} remains unchanged at concentrations from 0 to 5 mg/mL but is reduced dramatically at 10 mg/mL. The overall *PCE*

peaks at 17.0% with a Li-TFSI concentration of 5 mg/mL. The resistivity of spiro-OMeTAD HTL with different amounts of Li-TFSI dopants was measured using a 4-probe configuration (**Figure S2**). Assuming the only component changed in the solar cell is the HTL, the serial resistance (Rs) of the device is expected to change in proportion to the resistance of the HTLs. However, the Rs relationship to HTL resistivity is less straight-forward. Rs shows a rapid drop with increasing Li-TFSI concentration below 5 mg/mL, while the HTL resistance barely changed. When Li-TFSI is increased from 5 to 10 mg/mL, the HTL resistance dropped more significantly, yet the Rs remained almost unchanged. The incommensurate changes of Rs and HTL resistance suggest that HTL is not the only component changed in the solar cells when Li-TFSI dopant is added. It is likely that the Li^+-ion migration observed (**Figure 1**) is influencing other layers underneath the HTLs.

Table 1. Performance parameters of PSCs with different Li-TFSI amounts in HTL (reverse scan).

Li-TFSI (mg/mL)	J_{sc}(mA/cm^2)	V_{oc}(V)	*FF*	*PCE* (%)	Rs (Ω cm^2)	HTM resistivity (kΩ cm^{-1})
0	19.6±0.9	1.08±0.01	0.48±0.02	10.2±0.4	41.9	14.4
2.5	20.0±0.2	1.09±0.01	0.59±0.01	12.8±0.3	10.3	13.9
5.0	20.6±0.1	1.09±0.01	0.75±0.01	17.0±0.2	6.4	10.8
10.0	20.2±0.2	0.99±0.02	0.79±0.03	15.8±0.2	5.6	7.1

Besides the changes in device performance, more profound changes are found in the *J-V* hysteresis. The hysteresis effect is much more severe with higher concentration of Li-TFSI in HTLs. This could be seen both from the *J-V* scans in **Figure 2a** and extracted *PCE*s of forward and reverse scans in **Figure 2b**. The increased degree of hysteresis at higher Li-TFSI concentration suggests that Li^+ could be one factor contributing to the hysteresis phenomenon in PSCs.

To further verify that the observed performance and hysteresis changes are affected by the Li^+-ion migration (rather than just from the change of HTL), we compared two solar cells fabricated with the same Li-free HTL but following different fabrication approaches. Cell 1 was deposited with the Li-free HTL immediately after perovskite deposition. In Cell 2, the perovskite

layer was initially coated with Li-doped HTL and tested after finishing the Au electrodes (**Figure S3**). The Li-doped HTL and Au electrode were subsequently removed by soaking in chlorobenzene. Cell 2 was then re-deposited with the same Li-free HTL and Au electrode as Cell 1. Although the HTLs were identical, the two cells showed different *J-V* characteristics in **Figure 2d**, with Cell 2 having better *PCE* and *FF* as well as larger hysteresis. The difference could be explained by the processing history of Cell 2 as illustrated in **Figure 2c**. Li^+ ions (schematically illustrated using light green crosses) migrated to the perovskite and TiO_2 layer when Cell 2 was coated with Li-doped HTL. The migrated Li^+ ions remained in the perovskite and TiO_2 layers when the Li-doped HTL is removed using chlorobenzene. The residual Li^+ ions in Cell 2 improve the cell performance and show larger *J-V* hysteresis. The residual Li^+ ions in Cell 2 were also verified by induced coupled plasma-mass spectrometry (ICP-MS) as shown in **Table S1**. This suggests that the observed performance differences of solar cells with different Li^+ doping are more related to the migrating Li^+ ion, even though the changes of HTL properties cannot be completely ruled out.

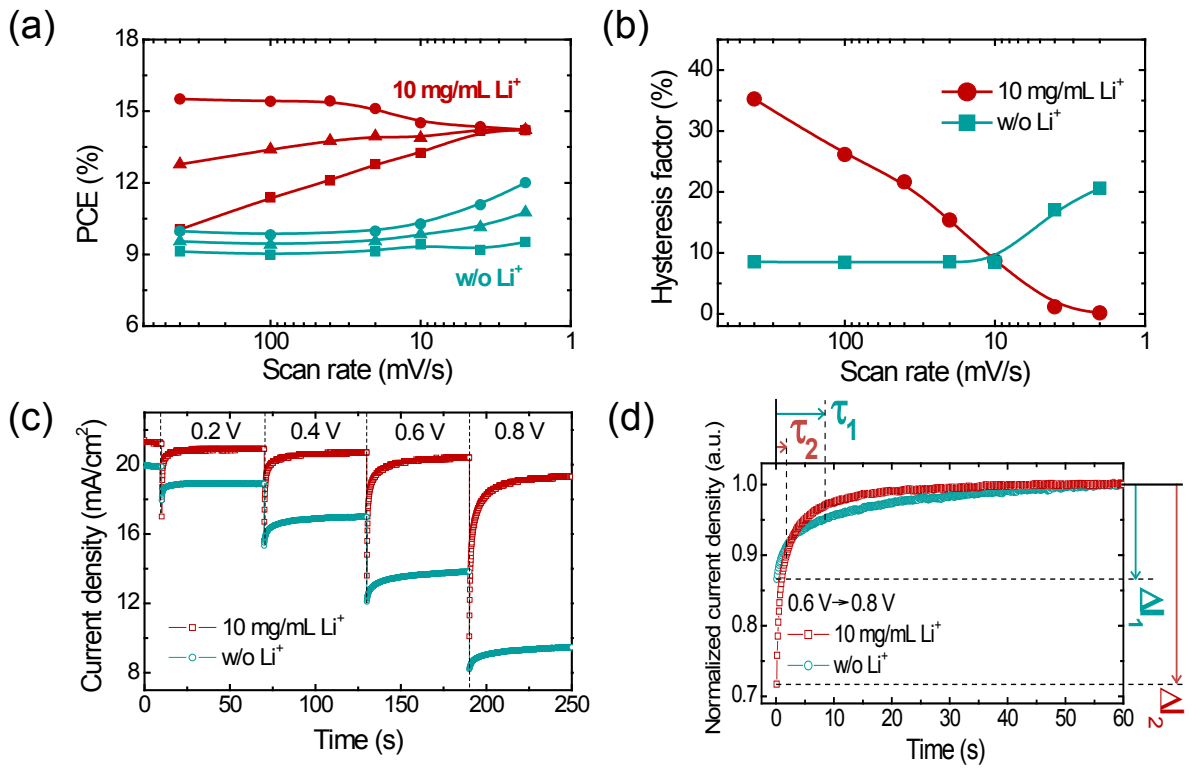

Figure 3. Hysteresis of solar cells with and without Li^+ in HTL. (a) *PCE* with forward (square) and reverse (circle) scan and the average *PCE* of forward and reverse scans (triangle); (b) Hysteresis factor of PSCs with and without Li-TFSI under different scan rate. Solid lines are guides to the eyes; (c) Photocurrents with stepping bias; (d) Normalized photocurrent with bias changed from 0.6 V to 0.8 V, showing different transition kinetics.

Figure 3a compares PCE of forward and reverse scan at different scan rates (*J-V* scan showed in **Figure S4**). For the purpose of discussion, we define hysteresis factor (*HF*) using the following expression:

$$Hysteresis\ factor = (PCE_{reverse}\text{-}PCE_{forward})/\ PCE_{reverse}. \quad (1)$$

The results for PSCs with and without Li^+ in HTL are compared in **Figure 3b**. The hysteresis effects in PSCs are usually reduced with slower scan speed.[26, 27] We observe a similar trend in the Li-containing cell. Starting with a large HF of 0.35 at 0.4 V/s, the forward and reverse *PCE*s converge to nearly identical value at a slow scan of 2 mV/s. In contrast, Li-free PSCs exhibit a different behavior. Their *HF* values remain small at about 0.08 with a wide scan range (400 to 10 m/s), and increase significantly at slower scan rates (*HF* = 0.17 at 4 mV/s; *HF* = 0.21 at 2 mV/s). This anomalous behavior suggests that the hysteresis for PSCs with and without Li dopants could be dominated by different factors.

Ion migrations and subsequent accumulations at the interfaces between perovskite and electron/hole transport layers have commonly been proposed as the main physical origin of the hysteresis phenomenon in PSCs.[27, 38-42] It is worth pointing out that most such studies (including both theoretical and experimental work) have focused only on the intrinsic ions (e.g., MA^+ or I^-) as the source causing the hysteresis, which is clearly evident. However, based on our TOF-SIMS observation of Li^+-ion migration as well as the distinct hysteresis behaviors in PSCs with and without the use of Li-TFSI in HTL, it is clear that the Li^+ migration in the Li-containing device also has a major contribution to the observed larger hysteresis effects compared to the Li-free devices. The ionic mobility of Li^+ in perovskite is expected to be higher than those intrinsic ions, given its smaller size. We hypothesize that the easy-migrating Li^+ ion in Li-containing cells introduces a large additional component to the hysteresis at fast scans and reaches a quasi-equilibrium state at slow scans. For Li-free devices, the intrinsic ions are "frozen" at relatively

fast scan rates where the devices show negligible hysteresis.[28] The intrinsic ions start to mobilize at slower scan rates and introduce hysteresis effects. Li^+ can have different diffusion mechanisms in the perovskite lattice compared to intrinsic ions. The different diffusion kinetics can explain the different rate dependences of hysteresis effects observed in PSCs with and without Li dopants (**Figures 3a and 3b**).

The different hysteresis behavior of PSCs with and without Li dopants is further illustrated from *J-V* scans shown with variable voltage steps in **Figures 3c and 3d**. When the cell experiences a sudden increase in bias, the photocurrent generally shows an initial drop, followed by an increasing transition to reach an equilibrium state. These transitions usually take seconds or even minutes in PSCs. *J-V* hysteresis is generally observed when the bias is scanned so fast that the photocurrent has not reached the equilibrium state at each scanning voltage before being recorded in their transitions states (lower in forward scans and higher in reverse scans). As illustrated in **Figure 3d**, the magnitude of photocurrent transition (ΔI) in the Li-containing device is larger than that in the Li-free device, but the transition is faster (i.e., time constant is smaller). The large ΔI of Li-containing cells causes large current differences between forward and reverse scans at fast scan rates, resulting in a large *J-V* hysteresis. The slower photocurrent transition kinetics in Li-free devices supports our hypothesis that intrinsic ions migrate at a slower rate than the Li^+-ion migration in Li-containing devices.

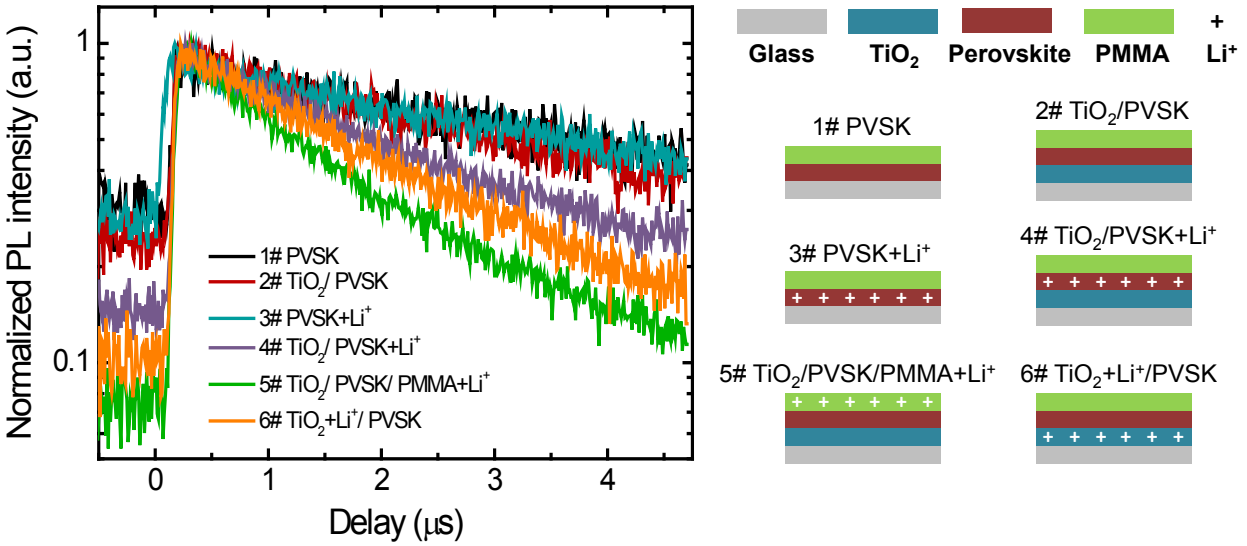

Figure 4. Time-resolved photoluminescence of perovskite with different layer-stacking configurations: 1, Perovskite/PMMA (black); 2, compact TiO_2/perovskite/PMMA (red); 3, Li-doped-perovskite/PMMA (blue); 4, TiO_2/Li-doped-perovskite/PMMA (purple); 5, TiO_2/perovskite/Li-doped-PMMA (green); and 6, Li-doped-TiO_2/perovskite/PMMA (orange).

For a planar PSC architecture using TiO_2 ETL, charge extraction from perovskite to TiO_2 is often not ideal and can also contribute to hysteresis behavior.[6, 47] Doping TiO_2 with lithium salt has been shown as one way to improve the charge injection from perovskite to TiO_2.[48, 49] To understand why Li doping in HTL can affect the hysteresis, we conducted TRPL measurements to examine the potential impact of Li^+-ion migration on charge extraction at the perovskite/TiO_2 interface. Perovskite thin films were deposited either on glass substrates or on glass with a sprayed TiO_2 compact layer. For all these samples, a 50-nm PMMA layer was coated on the perovskite layer to avoid degradation in ambient condition. The TRPL results are shown in **Figure 4** and the derived TRPL lifetimes are shown in **Table S2**. The laser pulse intervals were set to 10 μs. For certain samples with long PL lifetime, observable residual PL signal from previous laser pulses were imposed to the TRPL spectra and raised up the baseline. Perovskite deposited on the TiO_2 layer does not show a pronounced photoluminescence (PL) quenching compared to the pristine perovskite layer. It has been shown that TiO_2 itself did not efficiently extract electrons from perovskite and acted as a poor PL quencher in other studies.[50] The PL showed a substantially faster decay when TiO_2 was pre-doped with Li salt, with a lifetime of 2.8 μs for perovskite on pristine TiO_2 compared to 2.0 μs for perovskite on Li-doped TiO_2. Li doping modulates the perovskite/TiO_2 interface and facilitates electron injection from perovskite into TiO_2, leading to a stronger quenching effect. Interestingly, the better PL quenching is also observed when the Li salt is intentionally added to the perovskite layer or to the top PMMA coating layer when these samples are deposited on the TiO_2 layer. In contrast, when TiO_2 ETL is absent, a modest amount of Li doping in the perovskite (TOF-SIMS element analysis; **Figure S5**) does not show any noticeable effect on the PL lifetime, as shown in the PL transient of the Li-doped-perovskite/PMMA sample (labeled as PVSK+Li^+). Regardless of the specific layer doped with Li, the PL results all show faster decay when both Li and TiO_2 are present in the sample stacks (**Figure 4**). These results, especially with the TiO_2/perovskite/Li-doped-PMMA sample, strongly suggest that Li^+ ions migrate through the perovskite layer and modify the TiO_2 interface, facilitating carrier injection from perovskite to TiO_2. This enhancement of carrier extraction

assisted by the migrated Li^+ ions is consistent with the solar cell performance results, where higher *FF* and *PCE* were attained with higher Li-TFSI doping in the HTLs.

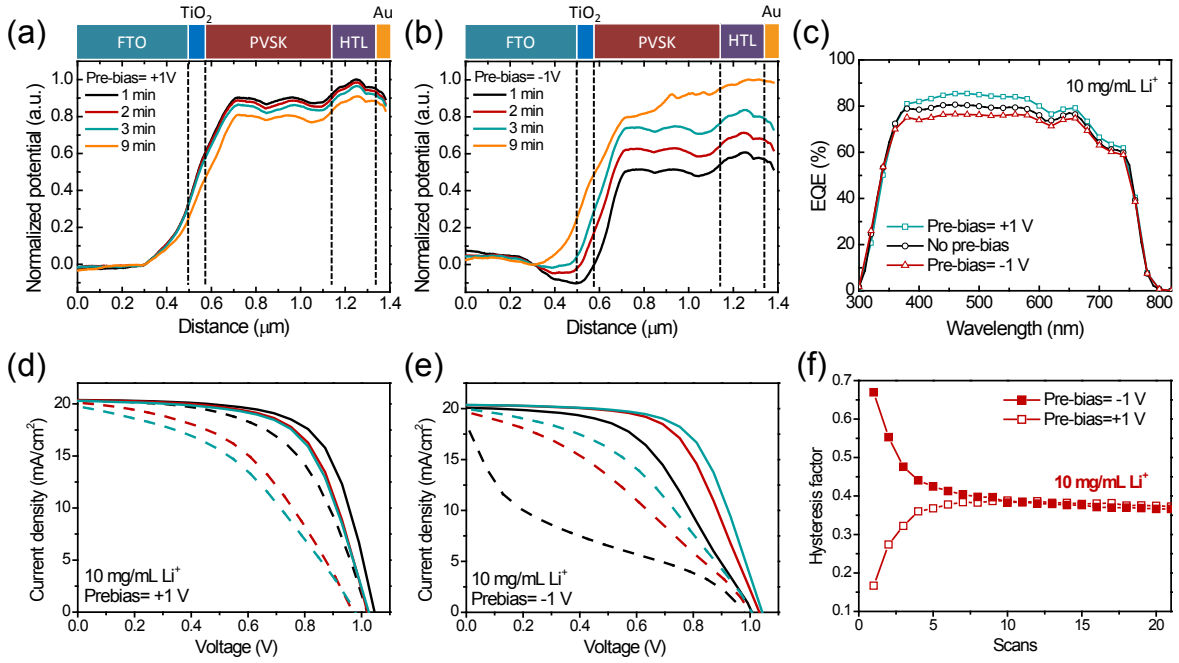

Figure 5. Modulations of PSC performance through Li^+-ion migrations induced by pre-bias poling. (a–b) Cross-sectional KPFM potentials after positive and negative poling; (c) EQE after pre-bias poling; (d–e) Forward (solid) and reverse (dash) *J-V* curves after pre-bias poling, 1st (black), 3rd (red), and 20th (blue) scans; (f) Hysteresis factor after pre-bias poling.

The Li^+-ion migration model can also be used to explain the solar cell performance changes after positive or negative pre-bias poling. Li^+ ions are driven toward or away from the TiO_2 interface under positive or negative external bias (the bias polarity is defined as follows: FTO/TiO_2 is grounded and bias is applied to HTL side, poling was taken under dark condition). The accumulation or removal of Li^+ at the TiO_2 surface modifies the charge-separation process at the perovskite/TiO_2 interfaces, thereafter affecting the overall performance of PSCs. Light soaking of PSC under open-circuit condition can be considered as holding the solar cell under a positive pre-bias, so the light soaking can also exhibit a pre-bias effect.[29] KPFM is a non-contact atomic force microscope technique to measure the surface potential distribution of materials in nm resolutions. KPFM of the cross-section of a PSC shows the potential profiles across different

layers in the PSCs and can provide information such as junction position and width of depletion region.[51] The KPFM potential line profiles in **Figures 5a and 5b** were measured at 0 V bias after the device was withdrawn from pre-bias at +1 V or at –1 V. The corresponding KPFM images were shown in **Figure S6**. The perovskite/TiO_2 interpenetration region was difficult to be resolved in the KPFM image due to the thin film thickness of mesoporous TiO_2 layer. For solar cell with 10-mg/mL Li-TFSI in spiro-OMeTAD, the potential drop was mainly seen at the TiO_2/perovskite interface, indicating a n-p junction structure.[51] The amount of potential drop at the n-p junction area is proportional to the local electric field. Larger potential drop indicates a stronger electric field and better charge separation at the particular interface. After being removed from the positive poling bias of +1 V, the electric field at TiO_2/perovskite interface is stronger initially but decreases gradually to an equilibrium state in several minutes. The potential change is more significant after –1 V negative poling. The electric field is weaker immediately after the poling with normalized potential drop about 0.6, but also gradually recovers to its steady state as the normalized potential drop increases to 0.8 after 9 minutes. This observation is consistent with our Li^+-ion migration models that Li^+ ions accumulate at the TiO_2 interface driven by the positive poling and facilitate the charge separation. Although negative poling sweeps Li^+ ions away from TiO_2 interface, the charge separation is hindered at the beginning but recoverable when Li^+ ions diffuse back to the equilibrium state. The change of charge-separation properties could also be seen from the EQE spectra of PSCs after poling (**Figure 5c**). The EQE spectra were taken at 0 V within 2 minutes after removing the pre-bias poling before the Li^+ ion could migrate back to the equilibrium state. The EQE responses are enhanced after positive pre-bias and reduced after negative pre-bias. These changes are seen across the entire photo-response wavelength range. The increase or decrease of EQE after poling is another piece of evidence that the change of carrier-separation efficiency is affected by Li^+-ion migration.

J-V hysteresis was also modulated by the pre-bias poling. The light *J-V* curves were measured repeatedly with forward and reverse scans after pre-bias poling, with each cycle taking about 6 seconds. **Figure 5d** shows the *J-V* scans with pre-condition of +1 V bias. After positive bias poling, Li^+ ions accumulate at the TiO_2 interface, leading to better carrier extraction and reduced interface recombination at the perovskite/TiO_2 interface. The device shows better *FF* and V_{oc} at the 1st scan than the subsequent scans. Also, the hysteresis is significantly suppressed in the 1st scan after positive poling. In contrast, with pre-condition of –1 V poling (**Figure 5e**),

the Li^+ ions are swept away from the TiO_2 interface, hindering the carrier extraction and increasing recombination. Consequently, lower V_{oc} and *FF* and large hysteresis are seen after the negative poling. In both cases, the *J-V* curves recover to a similar equilibrium state after about 10 repeated forward and reverse cycles. Hysteresis factors were calculated for each forward and reverse cycle and plotted in **Figure 5f**. The hysteresis intensity changes along with the redistribution of Li^+ ions in the devices. As pointed out by modeling result, hysteresis requires conditions of both ion migration and sequent changes in interface recombination.[39] After pre-bias of –1 V, the TiO_2 interface is relatively Li-poor and inefficient in charge extraction. The interface recombination rate shows more profound changes from local Li^+-ion movement driven by the forward and reverse scans, therefore resulting in a large *J-V* hysteresis (**Figure 5e**). For the pre-condition at +1 V bias, TiO_2 is preset to a Li-rich state with a reduced interface recombination; also the difference is trivial when Li^+ ions are moved in and out of TiO_2 layer by the external scanning bias. Therefore, the hysteresis effect is less serious. This is consistent with other reports showing suppressed hysteresis in the PSCs by doping TiO_2 with Li.[48, 49] The Li^+ ions in HTMs have also shown impacts on the stability of PSCs under continuous light soaking as shown in Figure S8. The Li-containing solar cells suffered more degradation in the V_{OC} and *FF* than the Li-free cells, indicating that the Li^+ ions might deteriorate the interfaces in the solar cells under continuous operation. Understanding the detailed degradation mechanism requires further investigations.

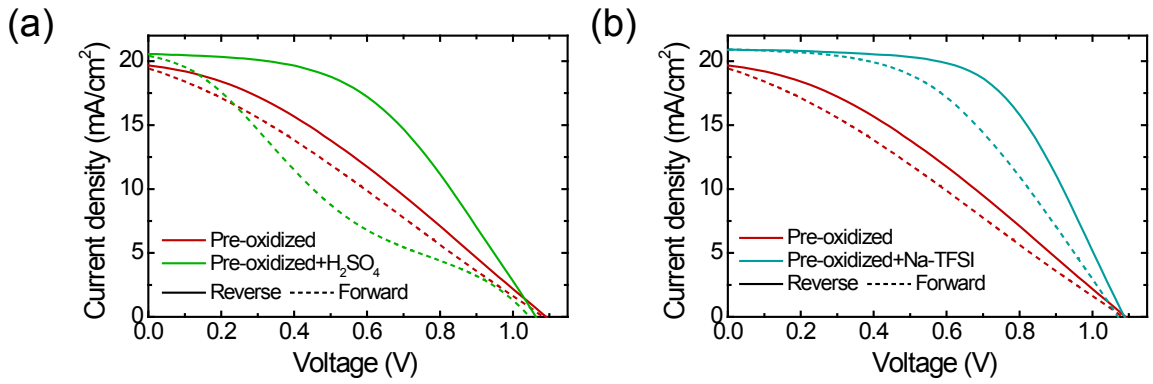

Figure 6. Performance of PSCs with dopants introducing other extrinsic ions in HTL. (a) H_2SO_4 as H^+ source; (b) Na-TFSI as Na^+ source.

Table 2. Performance of PSCs with different extrinsic ion dopants in HTL.

Dopants	Scan direction	J_{sc} (mA/cm^2)	V_{oc} (V)	*FF*	*PCE* (%)	Hysteresis factor
Pre-oxidized Spiro-OMeTAD	R	19.7	1.10	0.33	7.06	0.15
	F	19.4	1.08	0.29	5.99	
Pre-oxidized +H_2SO_4	R	20.6	1.06	0.48	10.45	0.56
	F	20.4	1.04	0.22	4.60	
Pre-oxidized +Na-TFSI	R	20.9	1.08	0.58	13.13	0.21
	F	20.9	1.08	0.46	10.36	

The significance of extrinsic ion migration on the PSCs was further examined by using extrinsic ions other than Li^+. **Figure 6** shows the impacts of extrinsic ions on the performance of PSCs using H^+ and Na^+ as examples. The reference cell was fabricated with pre-oxdized spiro-OMeTAD in the HTLs to avoid the extrinsic ion effects; it shows modest efficiency and hysteresis. H_2SO_4 and Na-TFSI were added to the HTL as the sources of H^+ and Na^+ ions. The solar cell performance parameters were summarized in **Table 2**. These results largely mimic Li^+; both these two ions enhance the *PCE* of solar cells at reverse scan, mainly through the improved *FF*. But the hysteresis between forward and reverse scan also became substantially larger with these extrinsic ions. The degree of the *PCE* improvement and the change in the hysteresis factor depends on the specific ions that have different migration kinetics and different impacts to the carrier collection interfaces. In this study, the extrinsic ions were only added through HTL dopants and the results clearly indicate that the Li^+ behavior is generalizable. There are other examples in the literature showing that alkaline halide dopant added in perovskite absorbers could lead to performance enhancement in PSCs.[52-54] The improvement has often been contributed to crystallography and morphology changes of the perovskite layers. However, our results raise the question of whether the extrinsic alkaline ion migration and modification of the carrier collection of the interfaces may also play a role in the efficiency improvements. Our study implies that the impact of extrinsic ion migration should be common to PSCs as well as other perovskite-related optoelectronic devices, with either ionic-doped contact layers or perovskite layers, and thus requires further investigation.

Conclusions

In summary, we have demonstrated extrinsic ion (e.g., Li^+, H^+, Na^+) migration in PSCs. We show that Li^+ ions in the HTL (spiro-OMeTAD) layer diffuse across the perovskite absorber layer and accumulate in the ETL (TiO_2) layer. The accumulation of Li^+ ions at the TiO_2 interface improves carrier injection from perovskite to TiO_2, and also increases the V_{oc} and *FF* in the Li-containing PSCs. Li-free and Li-containing solar cells show different hysteresis depending on scan rate, due to the different kinetics of extrinsic and intrinsic ion migrations. The migration of extrinsic Li^+ ions under bias can be used to explain the changes of KPFM, EQE, and *J-V* hysteresis under positive and negative pre-condition poling. We have further demonstrated that other extrinsic ions (such as H^+ and Na^+), when added to the HTL material, can also modulate the PSC performance and hysteresis. These results suggest that, like the intrinsic ion migration, extrinsic ion migration is also a general phenomenon in perovskite-based devices with significant impacts on the performance, hysteresis, and even degradation of the PSCs. The investigation of extrinsic ion migration behaviors in perovskite devices sheds new light on current research efforts focusing only on the intrinsic ion migrations, and would greatly deepen our understanding of their working mechanism and enable better device designs.

Acknowledgement

The work at the National Renewable Energy Laboratory is supported by the U.S. Department of Energy under Contract No. DE-AC36-08-GO28308. We acknowledge the support by the hybrid perovskite solar cell program of the National Center for Photovoltaics funded by the U.S. Department of Energy (DOE), Office of Energy Efficiency and Renewable Energy (EERE), Solar Energy Technologies Office (SETO). We thank Alan Sellinger for helpful discussion and providing materials. DK acknowledges the support from the DOE SunShot Initiative under the Next Generation Photovoltaics 3 program (DE-FOA-0000990). YY and MCB acknowledge the support from the Division of Chemical Sciences, Geosciences, and Biosciences, Office of Basic Energy Sciences (DOE). JAC was supported by the DOE/EERE Postdoctoral Research Award under the EERE/SETO administered by the Oak Ridge Institute for Science and Education (ORISE) for the DOE under DOE contract number DE-SC00014664. All opinions expressed in

this paper are the author's and do not necessarily reflect the policies and views of DOE, ORAU, or ORISE.

References

1 M. Saliba, T. Matsui, K. Domanski, J.-Y. Seo, A. Ummadisingu, S. M. Zakeeruddin, J.-P. Correa-Baena, W. R. Tress, A. Abate, A. Hagfeldt and M. Grätzel, *Science*, 2016.
2 W. S. Yang, J. H. Noh, N. J. Jeon, Y. C. Kim, S. Ryu, J. Seo and S. I. Seok, *Science*, 2015, **348**, 1234-1237.
3 Z.-K. Tan, R. S. Moghaddam, M. L. Lai, P. Docampo, R. Higler, F. Deschler, M. Price, A. Sadhanala, L. M. Pazos, D. Credgington, F. Hanusch, T. Bein, H. J. Snaith and R. H. Friend, *Nat. Nanotech.*, 2014, **9**, 687-692.
4 G. Xing, N. Mathews, S. S. Lim, N. Yantara, X. Liu, D. Sabba, M. Grätzel, S. Mhaisalkar and T. C. Sum, *Nat. Mater.*, 2014, **13**, 476-480.
5 L. Dou, Y. Yang, J. You, Z. Hong, W.-H. Chang, G. Li and Y. Yang, *Nat. Commun.*, 2014, **5**, 5404.
6 Y. Zhao and K. Zhu, *Chem. Soc. Rev.*, 2016, **45**, 655-689.
7 J. Gong, S. B. Darling and F. You, *Energy Environ. Sci.*, 2015, **8**, 1953-1968.
8 A. Kojima, K. Teshima, Y. Shirai and T. Miyasaka, *J. Am. Chem. Soc.*, 2009, **131**, 6050-6051.
9 H.-S. Kim, C.-R. Lee, J.-H. Im, K.-B. Lee, T. Moehl, A. Marchioro, S.-J. Moon, R. Humphry-Baker, J.-H. Yum, J. E. Moser, M. Grätzel and N.-G. Park, *Sci. Rep.*, 2012, **2**, 591.
10 NREL Solar Cell Efficiency Chart, http://www.nrel.gov/pv/assets/images/efficiency_chart.jpg, Accessed Dec. 2016.
11 S. De Wolf, J. Holovsky, S. J. Moon, P. Loper, B. Niesen, M. Ledinsky, F. J. Haug, J. H. Yum and C. Ballif, *J. Phys. Chem. Lett.*, 2014, **5**, 1035-1039.
12 S. D. Stranks, G. E. Eperon, G. Grancini, C. Menelaou, M. J. P. Alcocer, T. Leijtens, L. M. Herz, A. Petrozza and H. J. Snaith, *Science*, 2013, **342**, 341-344.
13 G. Xing, N. Mathews, S. Sun, S. S. Lim, Y. M. Lam, M. Grätzel, S. Mhaisalkar and T. C. Sum, *Science*, 2013, **342**, 344-347.
14 W.-J. Yin, T. Shi and Y. Yan, *Adv. Mater.*, 2014, **26**, 4653-4658.
15 J. Mizusaki, K. Arai and K. Fueki, *Solid State Ionics*, 1983, **11**, 203-211.
16 C. Eames, J. M. Frost, P. R. F. Barnes, B. C. O'Regan, A. Walsh and M. S. Islam, *Nat. Commun.*, 2015, **6**, 7497.

17 J. M. Azpiroz, E. Mosconi, J. Bisquert and F. De Angelis, *Energy Environ. Sci.*, 2015, **8**, 2118-2127.
18 J. Haruyama, K. Sodeyama, L. Han and Y. Tateyama, *J. Am. Chem. Soc.*, 2015, **137**, 10048-10051.
19 Y. Yuan, J. Chae, Y. Shao, Q. Wang, Z. Xiao, A. Centrone and J. Huang, *Adv. Energy Mater.*, 2015, **5**, 1500615-n/a.
20 T. Y. Yang, G. Gregori, N. Pellet, M. Gratzel and J. Maier, *Angew. Chem. Int. Ed.*, 2015, **54**, 7905-7910.
21 M. Bag, L. A. Renna, R. Y. Adhikari, S. Karak, F. Liu, P. M. Lahti, T. P. Russell, M. T. Tuominen and D. Venkataraman, *J. Am. Chem. Soc.*, 2015, **137**, 13130-13137.
22 M. N. F. Hoque, M. Yang, Z. Li, N. Islam, X. Pan, K. Zhu and Z. Fan, *ACS Energy Lett.*, 2016, **1**, 142-149.
23 Z. Xiao, Y. Yuan, Y. Shao, Q. Wang, Q. Dong, C. Bi, P. Sharma, A. Gruverman and J. Huang, *Nat. Mater.*, 2015, **14**, 193-198.
24 E. J. Yoo, M. Lyu, J.-H. Yun, C. J. Kang, Y. J. Choi and L. Wang, *Adv. Mater.*, 2015, **27**, 6170-6175.
25 C. Gu and J.-S. Lee, *ACS Nano*, 2016, **10**, 5413-5418.
26 H. J. Snaith, A. Abate, J. M. Ball, G. E. Eperon, T. Leijtens, N. K. Noel, S. D. Stranks, J. T. Wang, K. Wojciechowski and W. Zhang, *J. Phys. Chem. Lett.*, 2014, **5**, 1511-1515.
27 W. Tress, N. Marinova, T. Moehl, S. M. Zakeeruddin, M. K. Nazeeruddin and M. Grätzel, *Energy Environ. Sci.*, 2015, **8**, 995-1004.
28 E. L. Unger, E. T. Hoke, C. D. Bailie, W. H. Nguyen, A. R. Bowring, T. Heumuller, M. G. Christoforo and M. D. McGehee, *Energy Environ. Sci.*, 2014, **7**, 3690-3698.
29 C. Zhao, B. Chen, X. Qiao, L. Luan, K. Lu and B. Hu, *Adv. Energy Mater.*, 2015, **5**, 1500279.
30 R. Gottesman, E. Haltzi, L. Gouda, S. Tirosh, Y. Bouhadana, A. Zaban, E. Mosconi and F. De Angelis, *J. Phys. Chem. Lett.*, 2014, **5**, 2662-2669.
31 D. W. deQuilettes, W. Zhang, V. M. Burlakov, D. J. Graham, T. Leijtens, A. Osherov, V. Bulović, H. J. Snaith, D. S. Ginger and S. D. Stranks, *Nat. Commun.*, 2016, **7**, 11683.
32 E. T. Hoke, D. J. Slotcavage, E. R. Dohner, A. R. Bowring, H. I. Karunadasa and M. D. McGehee, *Chem. Sci.*, 2015, **6**, 613-617.
33 E. M. Sanehira, B. J. Tremolet de Villers, P. Schulz, M. O. Reese, S. Ferrere, K. Zhu, L. Y. Lin, J. J. Berry and J. M. Luther, *ACS Energy Lett.*, 2016, **1**, 38-45.
34 N.-G. Park, M. Grätzel, T. Miyasaka, K. Zhu and K. Emery, *Nat. Energy*, 2016, **1**, 16152.
35 J. Wei, Y. Zhao, H. Li, G. Li, J. Pan, D. Xu, Q. Zhao and D. Yu, *J. Phys. Chem. Lett.*, 2014, **5**, 3937-3945.
36 V. W. Bergmann, S. A. L. Weber, F. Javier Ramos, M. K. Nazeeruddin, M. Grätzel, D. Li, A. L. Domanski, I. Lieberwirth, S. Ahmad and R. Berger, *Nat. Commun.*, 2014, **5**, 5001.
37 B. Chen, M. Yang, X. Zheng, C. Wu, W. Li, Y. Yan, J. Bisquert, G. Garcia-Belmonte, K. Zhu and S. Priya, *J. Phys. Chem. Lett.*, 2015, **6**, 4693-4700.
38 H. Yu, H. Lu, F. Xie, S. Zhou and N. Zhao, *Adv. Funct. Mater.*, 2016, **26**, 1411-1419.
39 S. van Reenen, M. Kemerink and H. J. Snaith, *J. Phys. Chem. Lett.*, 2015, **6**, 3808-3814.
40 P. Calado, A. M. Telford, D. Bryant, X. Li, J. Nelson, B. C. O'Regan and P. R. F. Barnes, *Nat. Commun.*, 2016, **7**, 13831.

41 M. De Bastiani, G. Dell'Erba, M. Gandini, V. D'Innocenzo, S. Neutzner, A. R. S. Kandada, G. Grancini, M. Binda, M. Prato, J. M. Ball, M. Caironi and A. Petrozza, *Adv. Energy Mater.*, 2016, **6**, 1501453.
42 C. Li, S. Tscheuschner, F. Paulus, P. E. Hopkinson, J. Kiessling, A. Kohler, Y. Vaynzof and S. Huettner, *Adv Mater*, 2016, **28**, 2446-2454.
43 H. R. Xia, W. T. Sun and L. M. Peng, *Chem Commun*, 2015, **51**, 13787-13790.
44 G. Armstrong, A. R. Armstrong, P. G. Bruce, P. Reale and B. Scrosati, *Adv. Mater.*, 2006, **18**, 2597-2600.
45 K. Zhu, Q. Wang, J.-H. Kim, A. A. Pesaran and A. J. Frank, *J. Phys. Chem. C*, 2012, **116**, 11895-11899.
46 W. H. Nguyen, C. D. Bailie, E. L. Unger and M. D. McGehee, *J. Am. Chem. Soc.*, 2014, **136**, 10996-11001.
47 G. Xing, B. Wu, S. Chen, J. Chua, N. Yantara, S. Mhaisalkar, N. Mathews and T. C. Sum, *Small*, 2015, **11**, 3606-3613.
48 J. H. Heo, M. S. You, M. H. Chang, W. Yin, T. K. Ahn, S.-J. Lee, S.-J. Sung, D. H. Kim and S. H. Im, *Nano Energy*, 2015, **15**, 530-539.
49 F. Giordano, A. Abate, J. P. Correa Baena, M. Saliba, T. Matsui, S. H. Im, S. M. Zakeeruddin, M. K. Nazeeruddin, A. Hagfeldt and M. Graetzel, *Nat Commun*, 2016, **7**, 10379.
50 R. Ihly, A.-M. Dowgiallo, M. Yang, P. Schulz, N. J. Stanton, O. G. Reid, A. J. Ferguson, K. Zhu, J. J. Berry and J. L. Blackburn, *Energy Environ. Sci.*, 2016, **9**, 1439-1449.
51 C.-S. Jiang, M. Yang, Y. Zhou, B. To, S. U. Nanayakkara, J. M. Luther, W. Zhou, J. J. Berry, J. van de Lagemaat, N. P. Padture, K. Zhu and M. M. Al-Jassim, *Nat. Commun.*, 2015, **6**, 8397.
52 K. M. Boopathi, R. Mohan, T.-Y. Huang, W. Budiawan, M.-Y. Lin, C.-H. Lee, K.-C. Ho and C.-W. Chu, *J. Mater. Chem. A*, 2016, **4**, 1591-1597.
53 J. Chang, Z. Lin, H. Zhu, F. H. Isikgor, Q.-H. Xu, C. Zhang, Y. Hao and J. Ouyang, *J. Mater. Chem. A*, 2016, **4**, 16546-16552.
54 Y. Sheng, Y. Hu, A. Mei, P. Jiang, X. Hou, M. Duan, L. Hong, Y. Guan, Y. Rong, Y. Xiong and H. Han, *J. Mater. Chem. A*, 2016, **4**, 16731-16736.